

# Iron-impregnated biochars as effective phosphate sorption materials

Barbora Micháleková-Richveisová<sup>1</sup> · Vladimír Frišták<sup>2</sup> · Martin Pipiška<sup>3</sup> ·  
Libor Ďuriška<sup>4</sup> · Eduardo Moreno-Jimenez<sup>5</sup> · Gerhard Soja<sup>2</sup>

Received: 1 December 2015 / Accepted: 3 October 2016 / Published online: 11 October 2016  
© Springer-Verlag Berlin Heidelberg 2016

**Abstract** A new post-treatment method was applied for improving the sorption efficiency of biochar-based sorbents for anionic forms of phosphorus. The Fe-impregnation through direct hydrolysis of  $\text{Fe}(\text{NO}_3)_3$  was used to produce impregnated corn cob- (IBC A), garden wood waste- (IBC B), and wood chip-derived biochars (IBC C). The qualitative and quantitative effects of impregnation process on biochars were confirmed by SEM-EDX, FTIR, and ICP-MS. The analyses revealed increased concentrations of N and thus potential  $\text{NO}_3^-$  participation in the phosphate sorption process. Biochar surface area showed a significant decrease after the impregnation process due to the filling of micro- and mesopores with Fe maximum sorption capacity ( $Q_{\text{max}}$ ) increased by a factor of 12–50. The sorption processes of phosphates by IBC A, IBC B, and IBC C were dependent on pH, initial concentration, and time. Speciation analysis and pH-study confirmed the range of pH 4.5–5.5 as optimum values at which most of phosphorus is present in form of mononuclear  $\text{H}_2\text{PO}_4^-$ . Batch sorption

experiments showed a significant increase in the sorption capacity for phosphates by Fe impregnation of biochar as well as effectiveness and stability of this treatment. These findings indicate an option for utilizing engineered biochars as tools for the recovery of phosphorus from the aquatic environment.

**Keywords** Phosphates · Biochar · Impregnation · Sorption isotherms · Fe modification

## Introduction

Phosphorus, sometimes referred to as the element of the twenty-first century, represents a burning issue in environmental management. Eutrophication has become a serious environmental problem in surface waters around the world. Elevated phosphorus concentration in surface waters and phosphate exchange between water and sediments are important processes affecting growth of algae and macrophytes. For this reason, eutrophication caused either by runoff from agricultural areas or by waste water input into receiving waters has to be controlled. The exchange of phosphates between the solid and liquid phase involves a number of complex processes. One of them is the removal of dissolved phosphate from the water column through sorption by the sediments (Wang et al. 2015). For this reason, the phosphate sorption characteristics are important for the interpretation of phosphate exchange between sediments and water. The reactivity of phosphorus is a function of the charge of the mineral surfaces present in the fraction, the redox status, and pH value. Fe, Al, and Mg oxyhydroxide particles will adsorb P at low pH, whereas as pH increases, the negative surface charge of soil particles predominates and repels the phosphate oxyanions (Sharpley et al. 2000).

Responsible Editor: Philippe Garrigues

✉ Vladimír Frišták  
fristak.vladimir.jr@gmail.com

- <sup>1</sup> Department of Ecochemistry and Radioecology, University of SS. Cyril and Methodius, J. Herdu 2, Tmava 917 01, Slovak Republic
- <sup>2</sup> Energy Department, Austrian Institute of Technology GmbH, 3430 Tulln, Austria
- <sup>3</sup> Department of Chemistry, Tmava University, Tmava 91701, Slovak Republic
- <sup>4</sup> Faculty of Materials Science and Technology in Tmava, Slovak University of Technology in Bratislava, Paulínska 16, Tmava 917 24, Slovak Republic
- <sup>5</sup> Departamento de Química Agrícola y Bromatología, Universidad Autónoma de Madrid, 28049 Madrid, Spain

Biochar represents low-density charred material produced by heating organic feedstocks under anoxic conditions and temperatures of 300–1000 °C (Lehmann and Joseph 2015). A wide range of biomass materials such as agricultural residues and by-products of food processing, animal manure, and wood residues can be utilized for biochar production. This pyrolysis product is used in many agro-environmental applications such as soil amendment and as immobilization tool for a wide range of inorganic and organic xenobiotics such as heavy metals, metalloids, or polycyclic aromatic hydrocarbons (Moreno-Castilla 2004; Martin et al. 2012; Ahmad et al. 2014; Hu et al. 2015). Furthermore, biochar application improves soil fertility by altering several physicochemical properties of soil such as bulk density, water holding capacity, specific surface area, pH, and cation exchange capacity (Novak et al. 2009; Laird et al. 2010; Kloss et al. 2012; Tang et al. 2013). The sorption properties of biochar determine the suitability of this material as an efficient tool in remediation studies. The sorption of cationic forms of pollutants such as heavy metals has already been discussed in earlier studies (Frišták et al. 2014, 2015; Kolodynska et al. 2012). For anionic forms, the existing information gap remains to be filled. The negative surface charge of non-modified biochar causes non-attraction or only very weak interactions with phosphates. Based on this scenario, a modification of biochar surfaces and structure is required. Therefore, various modified biochar types have been developed and applied for water treatment (Hu et al. 2015; Agrafioti et al. 2014; Zeng et al. 2013). Functional additives (such as  $\text{AlCl}_3$ ,  $\text{MgCl}_2$ , and  $\text{Fe}_3\text{O}_4$ ) have been used for improving the sorption and surface properties of biochar in order to better adsorb phosphate oxyanions (Zhang and Gao 2013; Wang et al. 2015). Positively charged surface area can increase the biochar sorption capacity for  $\text{PO}_4^{3-}$ . Hu et al. (2015) used direct hydrolysis of iron salt to produce Fe-impregnated biochar in order to improve sorption ability to As from aqueous solution. Similar findings were observed by Zhang and Gao (2013). Steam activation of biochar accelerated nutrient retention and uptake by plants relative to non-activated biochar (Borchard et al. 2012). Chen et al. (2011) prepared three magnetic biochars by chemical coprecipitation of  $\text{Fe}^{3+}/\text{Fe}^{2+}$  on raw material of orange peel powder and pyrolyzed it under different temperature conditions. All these studies showed that biochar needs to be treated for specific purposes in order to achieve the optimal environmental services.

In this work, the effect of chemical post-treatment of biochar on phosphate sorption is discussed. The main objective of this work was to analyze the sorption mechanisms of phosphates ( $\text{PO}_4^{3-}$ ) onto unimpregnated and Fe-impregnated biochar produced from three different feedstocks.

## Materials and methods

### Biochar preparation and modification

Biochar samples were produced by slow pyrolysis from three different feedstocks: corn cobs (BC A), garden wood waste (BC B), and wood chips (BC C). Raw materials were pyrolyzed at 500 °C at a residence time 120 min in a rotary furnace. For ensuring oxygen-free environment and uniform heating conditions, nitrogen was used as flush gas. After pyrolysis, biochar samples were ground and sieved to achieve particle size 0.5–1 mm. Sorbents were rinsed several times by deionized water ( $<0.4 \mu\text{S cm}^{-1}$ ).

Fe-impregnation was provided by direct hydrolysis of  $\text{Fe}(\text{NO}_3)_3$  (Reaction (1)):



For impregnation, 100 g of biochar was mixed with iron nitrate solution for 12 h using a magnetic stirrer and then dried at 105 °C for 12 h. The dried composites were rinsed several times with deionized water ( $<0.4 \mu\text{S cm}^{-1}$ ) in order to remove formed surface iron hydroxide, and then dried overnight at 105 °C. The resulting products Fe-impregnated BC A (IBC A), Fe-impregnated BC B (IBC B), and Fe-impregnated BC C (IBC C) were sieved to obtain a particle size 0.5–1 mm and stored at 22 °C in polypropylene boxes for sorption experiments.

### Sorbent characterization

The total contents of C, H, and N in biochar samples were determined using a CHN Elemental Analyzer (CHNS-O EA 1108, Carlo Erba Instruments, Italy). Total Fe and P concentrations in biochar were determined using ICP-MS (Perkin Elmer, Elan DRCe 9000, USA) after wet digestion with  $\text{HNO}_3$  and  $\text{H}_2\text{O}_2$  (Enders and Lehmann 2012). P content in biochar digests was confirmed colorimetrically by malachite green microplate UV-VIS method. Readily soluble Fe was determined in deionized water extracts ( $w/v$  1/30) after 24 h shaking by ICP-MS. Specific surface areas of the samples were measured by methylene blue sorption method according to Nunes and Guerreiro (2011) and the technique of nitrogen adsorption and desorption (SORPTOMATIC 1990, Italy) followed by the Brunauer-Emmett-Tellers (BET) model evaluation. The active and potential pH values of samples were measured after mixing samples with deionized water and 1.0 mol  $\text{L}^{-1}$  KCl (1/15  $w/v$ ) for 1 and 1 h of stabilization. Electrical conductivities (EC) of samples were measured in deionized water (1/10  $w/v$ ) after 24 h of mixing. Anion

exchange capacities (AEC) were determined using bromide as index anion according Lawrinenko (2014). Carbonate equivalents were determined by the Scheibler method (Puschenreiter et al. 2013). The sorbent surface functional groups were characterized by spectral analysis in infrared region with Fourier transformation (FTIR) (Perkin Elmer Spectrum System 2000, USA). The samples were prepared in KBr with ratio 1:200 (biochar:KBr) and pressed into pellets. The spectra were collected in the mid-infrared from 4000 to 400 cm<sup>-1</sup>, in transmission mode, using 4 cm<sup>-1</sup> spectral resolution and 64 accumulations for each collection. The spectra were corrected against a pure KBr pellet and the surrounding air as a background spectrum without smoothing. Obtained data were evaluated by software Spectrum and MicroCal Origin 8.0 Professional (OriginLab Corporation, Northampton, USA). The intra-structures of Fe-impregnated sorbents and surface structure analysis were observed by scanning electron microscopy (SEM) coupled with electron dispersive X-ray microanalyses (EDX) using electron microscope JEOL JSM7600F (Japan). The analyses were performed at a voltage of 20 kV, vacuum pressure 9.0 × 10<sup>-4</sup> Pa, and the magnifications 250×, 500×, and 1000×.

**Determination of readily soluble PO<sub>4</sub><sup>3-</sup>**

The unimpregnated and Fe-impregnated biochars were shaken in polypropylene centrifuge tubes with deionized water (w/v 1/30) for 24 h. Sediments were separated from liquids by centrifugation (4000 min<sup>-1</sup>, 10 min) and filtered by 0.45-μm syringe filters. The supernatants were tested for P-PO<sub>4</sub><sup>3-</sup> content by anion chromatography (IC, Dionex® 1100 ion chromatograph with a conductivity detector ASRS 300, 4 mm). Filters and tubes were tested for PO<sub>4</sub><sup>3-</sup> retained before each use.

**PO<sub>4</sub><sup>3-</sup> sorption process optimization**

The sorption process of PO<sub>4</sub><sup>3-</sup> from single-component system was studied using a batch equilibration method according to the OECD guideline no. 106 (OECD, 2001) modified by Frišták et al. (2015).

**Effect of reaction time**

Sorption kinetic experiments were carried out by suspending 0.5 g of unimpregnated and impregnated sorbents in 15 mL of 65 mg L<sup>-1</sup> PO<sub>4</sub><sup>3-</sup> (form K<sub>2</sub>HPO<sub>4</sub>) and shaken at 150 min<sup>-1</sup>, 24 ± 2 °C, for the time periods 5, 10, 60, 120, 240, 360, 1440, and 2880 min. The concentrations of unsorbed PO<sub>4</sub><sup>3-</sup> in aliquots after centrifugation (4000 min<sup>-1</sup>, 5 min) and filtration by

0.45-μm syringe filters were determined by IC. Retention of filters for PO<sub>4</sub><sup>3-</sup> was tested before each use.

Sorption of PO<sub>4</sub><sup>3-</sup> was calculated according to Eq.2:

$$Q_{eq} = (C_0 - C_{eq}) \times V/w, \tag{2}$$

where  $Q_{eq}$  is PO<sub>4</sub><sup>3-</sup> uptake (mg g<sup>-1</sup>),  $C_0$  is the initial liquid-phase concentrations of PO<sub>4</sub><sup>3-</sup> (mg L<sup>-1</sup>),  $C_{eq}$  is the equilibrium liquid-phase concentrations of PO<sub>4</sub><sup>3-</sup> (mg L<sup>-1</sup>),  $V$  is the volume (L), and  $w$  is the amount of biochar (g).

**Kinetic models**

For investigation of sorption kinetics, the models of pseudo-first order, pseudo-second order, and Azizian pseudo- $n$  order were used. Parameters of kinetic models were obtained by using the program MicroCal Origin 8.0 Professional (OriginLab Corporation, Northampton, USA). The pseudo-first order equation (Lagergren equation) can be defined as

$$dQ_t/dt = k_1 (Q_{eq} - Q_t), \tag{3}$$

in which  $Q_t$  is the amount of PO<sub>4</sub><sup>3-</sup> sorbed at time  $t$  (mg g<sup>-1</sup>),  $Q_{eq}$  is its value at equilibrium (mg g<sup>-1</sup>), and  $k_1$  is the rate constant of pseudo-first order process (min<sup>-1</sup>).

The pseudo-second order model can be defined as

$$\frac{dQ_t}{dt} = k_2 (Q_{eq} - Q_t)^2, \tag{4}$$

in which  $k_2$  is the rate constant of the pseudo-second order process (g mg<sup>-1</sup> min<sup>-1</sup>) and  $Q_t$  and  $Q_{eq}$  have the same meaning as in the pseudo-first order equation.

Pseudo- $n$  order model according Azizian and Fallah (2010) can be defined as

$$\frac{dQ_t}{dt} = k_3 \frac{Q_{eq}^n - Q_t^n}{Q^{n-1}}, \tag{5}$$

in which  $k_3$  is the rate constant of the pseudo- $n$  order process (g mg<sup>-1</sup> min<sup>-1</sup>),  $n$  is the order of rate equation, and  $Q_t$  and  $Q_{eq}$  have the same meaning as in the pseudo-first order equation.

**Effect of PO<sub>4</sub><sup>3-</sup> initial concentration**

The adsorption isotherms were investigated in the concentration range of 10–200 mg L<sup>-1</sup> PO<sub>4</sub><sup>3-</sup> at 24 ± 2 °C. Using 0.5 mg biochar, 15 mL solution with varying concentrations of PO<sub>4</sub><sup>3-</sup> were added. After shaking at 200 min<sup>-1</sup>, 24 ± 2 °C for 24 h, the samples were separated by centrifugation (4000 min<sup>-1</sup>,

5 min) and filtration was performed as in kinetic studies. Concentrations of  $\text{PO}_4^{3-}$  in liquid phase were measured by IC. Sorptions of  $\text{PO}_4^{3-}$  were calculated according to Eq. 2.

### Adsorption isotherms

The obtained equilibrium sorption data were analyzed by mathematical equations of adsorption models with the terms of Langmuir, Freundlich, and Dubinin-Kaganer-Radushkevich (DKR). Parameters of adsorption isotherms were calculated by non-linear regression analysis using the program MicroCal Origin 8.0 Professional (OriginLab Corporation, Northampton, USA).

Langmuir is the simplest type of theoretical adsorption model. The isotherm is given by the following equation:

$$Q_{eq} = (bQ_{max}C_{eq}) / (1 + bC_{eq}), \quad (6)$$

where  $Q_{eq}$  is the amount of sorbed  $\text{PO}_4^{3-}$  at equilibrium ( $\text{mg g}^{-1}$ ),  $b$  is the isotherm coefficient characterizing biochar affinity to  $\text{PO}_4^{3-}$  ions in solution ( $\text{L mg}^{-1}$ ),  $Q_{max}$  is the maximum sorption capacity at saturated biochar binding sites ( $\text{mg g}^{-1}$ ), and  $C_{eq}$  represents  $\text{PO}_4^{3-}$  equilibrium concentration in solution ( $\text{mg L}^{-1}$ ).

The Freundlich adsorption model is commonly used to describe the adsorption process on heterogeneous surface. The isotherm is given by the following equation:

$$Q_{eq} = KC_{eq}^{(1/n)} \quad (7)$$

where  $Q_{eq}$  is the amount of sorbed  $\text{PO}_4^{3-}$  at equilibrium ( $\text{mg g}^{-1}$ ),  $K$  and  $n$  are the Freundlich empirical constants characterizing parameters and intensity of sorption process ( $\text{L g}^{-1}$ ), and  $C_{eq}$  is  $\text{PO}_4^{3-}$  equilibrium concentration in solution ( $\text{mg L}^{-1}$ ).

The Dubinin-Kaganer-Radushkevich (DKR) model is shown to be more general than the Langmuir and Freundlich isotherms. The DKR model has the following linear form:

$$\ln Q_{eq} = \ln Q_m - \beta \varepsilon^2, \quad (8)$$

where  $Q_m$  is  $\text{PO}_4^{3-}$  monolayer maximum sorption capacity,  $\beta$  is the activity coefficient related to mean sorption energy, and  $\varepsilon$  is the Polanyi potential, which is equal to

$$\varepsilon = RT \ln(1 + 1/C_{eq}), \quad (9)$$

where  $R$  is the gas constant ( $\text{J mol}^{-1} \text{K}^{-1}$ ) and  $T$  is the temperature (K).

### Effect of reaction pH

To determine the effect of pH on phosphate sorption, 0.5 g of impregnated or unimpregnated biochar sample was mixed with 15 mL of phosphate solution ( $150 \text{ mg L}^{-1} \text{PO}_4^{3-}$ ) with a pH value from 3 to 8. To achieve the required pH,  $1.0 \text{ mol L}^{-1} \text{HCl}$  and  $1.0 \text{ mol L}^{-1} \text{NaOH}$  were added. The samples were shaken at  $200 \text{ min}^{-1}$ ,  $24 \pm 2 \text{ }^\circ\text{C}$  for 24 h, to reach sorption equilibrium. After centrifugation ( $4000 \text{ min}^{-1}$ , 5 min) and filtration, the concentrations of unsorbed  $\text{PO}_4^{3-}$  in liquid phase by IC were measured. Sorptions of  $\text{PO}_4^{3-}$  were calculated according to Eq. 2.

### Phosphorus speciation

Calculation of P speciation in aqueous solution as a function of total salt concentration, stability constants, and solution pH was performed using the Visual Minteq program (version 2.52). Visual Minteq works with an extensive thermodynamic database for the calculation of metal speciation, solubility, and equilibrium (Gustafsson 2013). Data were calculated considering the carbonate system naturally in equilibrium with atmospheric  $\text{CO}_2$  ( $p(\text{CO}_2) = 38.5 \text{ Pa}$ ).

## Results and discussion

### Characterization of biochar

Physicochemical characterization of unimpregnated and Fe-impregnated samples revealed the main effect of chemical modification via hydrolysis by significant changes of biochar properties (Table 1). The change of surface structure and the strong protonation of binding sites by  $\text{H}^+$  ions caused a pH decrease in all three impregnated forms. Comparison of EC values showed significant effect of feedstock chemical composition on conductivity of pyrolyzed materials. The values of EC decreased in order  $\text{BC A} > \text{BC B} > \text{BC C}$ . The effect of Fe impregnation revealed higher values of EC in the case of IBC B and IBC C compared to unimpregnated samples. IBC A showed lower EC value compared to BC A as an agricultural waste-derived biochar rich on soluble salts removed during impregnation process. Hydrolysis and subsequent uptake of free  $\text{NO}_3^-$  by biochars reflect the increasing of anionic exchange capacities of IBC A, IBC B, and IBC C samples compared to unimpregnated biochars. This fact is also clear from the elevated total N content determined in impregnated samples (Table 1). Similar results were observed by Hu et al. (2015). Additionally, elemental analysis showed a reduction of total C contents by  $>10 \%$  in IBC A,  $>2 \%$  in IBC B, and  $>12 \%$  in IBC C. A similar trend was confirmed by carbonate losses in biochar after impregnation. Removal of inorganic C forms during acid hydrolysis of biochars and increased



**Table 1** Physicochemical properties of unimpregnated (BC A, BC B, and BC C) and impregnated (IBC A, IBC B, and IBC C) biochars. All measurements were done in triplicates (±SD)

	Unimpregnated			Impregnated		
	BC A	BC B	BC C	IBC A	IBC B	IBC C
pH (H <sub>2</sub> O)	8.74 ± 0.07	9.9 ± 0.00	8.58 ± 0.01	3.38 ± 0.05	3.83 ± 0.01	3.67 ± 0.01
EC (mS cm <sup>-1</sup> )	2.39 ± 0.01	1.15 ± 0.02	0.36 ± 0.01	1.43 ± 0.01	2.31 ± 0.02	1.13 ± 0.03
AEC (cmol kg <sup>-1</sup> )	<0.50	<0.50	<0.50	1.22 ± 0.25	3.92 ± 0.16	1.72 ± 0.15
SA (m <sup>2</sup> g <sup>-1</sup> )	16.20 ± 0.45	23.27 ± 0.56	26.42 ± 0.58	6.19 ± 0.21	9.42 ± 0.47	11.08 ± 0.78
C%	82.82 ± 1.17	80.45 ± 1.02	79.87 ± 1.45	74.2 ± 1.29	78.74 ± 1.28	69.84 ± 1.17
H%	2.08 ± 0.12	1.64 ± 0.08	1.59 ± 0.08	1.64 ± 0.04	1.89 ± 0.07	1.28 ± 0.02
N%	1.39 ± 0.07	0.65 ± 0.03	0.45 ± 0.02	1.56 ± 0.04	1.57 ± 0.07	2.42 ± 0.11
S%	0.19 ± 0.01	0.13 ± 0.01	0.18 ± 0.01	0.19 ± 0.01	0.13 ± 0.01	0.18 ± 0.01
C/N ratio	59.58	123.77	177.49	30.66	50.47	44.48
CaCO <sub>3</sub> (%)	2.82 ± 0.05	6.60 ± 0.25	0.65 ± 0.02	0.3 ± 0.01	1.1 ± 0.02	0.6 ± 0.01
Total P (mg g <sup>-1</sup> )	3.24 ± 0.15	6.05 ± 0.21	2.11 ± 0.15	2.74 ± 0.04	1.52 ± 0.03	0.56 ± 0.01
Readily soluble PO <sub>4</sub> <sup>3-</sup> (mg g <sup>-1</sup> )	0.43 ± 0.01	0.49 ± 0.01	0.06 ± 0.01	<0.05	<0.05	<0.05
Total Fe (mg g <sup>-1</sup> )	0.65 ± 0.02	1.87 ± 0.03	0.58 ± 0.01	21.85 ± 1.21	39.46 ± 2.14	18.87 ± 0.78
Readily soluble Fe (mg g <sup>-1</sup> )	<0.05	<0.05	<0.05	0.06 ± 0.01	0.15 ± 0.01	0.35 ± 0.01

concentrations of total N and Fe represent the main contributions to explain differences in total C contents revealed in materials before and after impregnation process.

Determination of surface areas (SA) showed values in the range 16.20–26.42 m<sup>2</sup> g<sup>-1</sup> for unimpregnated and 6.19–11.08 m<sup>2</sup> g<sup>-1</sup> for impregnated samples. Decreased SA values of impregnated biochars suggest that Fe impregnation filled up the pores present on the biochar samples. Therefore, SA cannot be considered as the key parameter in determining phosphate sorption onto biochar (Galamboš et al. 2015; Hu et al. 2015). Fe contents of BC A, BC B, and BC C were 0.65, 1.87, and 0.58 mg g<sup>-1</sup>, respectively. Fe-impregnated biochars derived from corn cobs (IBC A), garden wood waste (IBC B), and wood chips (IBC C) contained 21.85, 39.46, and 18.87 mg g<sup>-1</sup>. These values confirm effectivity of biochar impregnation by iron particles.

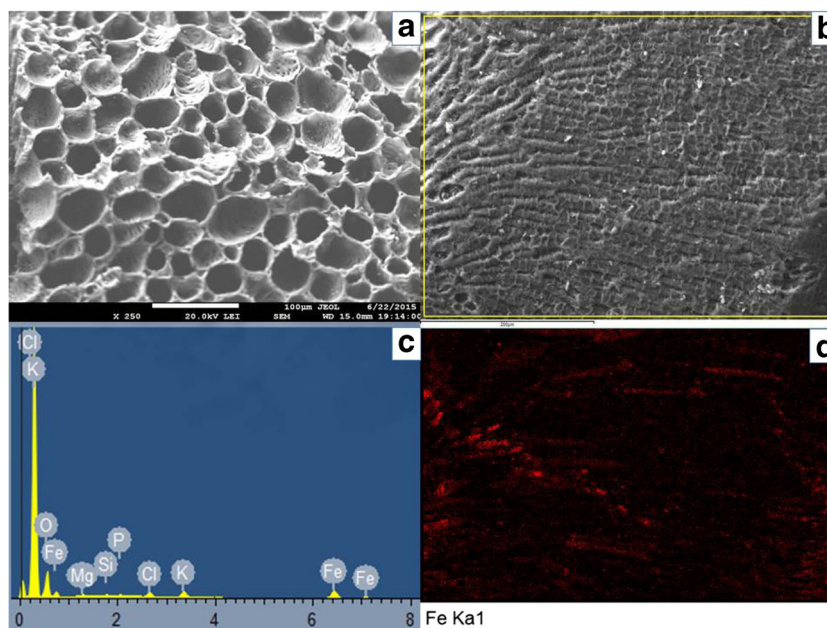
In order to determine the releases of readily soluble PO<sub>4</sub><sup>3-</sup> from unimpregnated and impregnated biochars, they were extracted by deionized water. Results showed that PO<sub>4</sub><sup>3-</sup> can be released by 24 h extraction in amount of 0.43 mg g<sup>-1</sup> from BC A, 0.49 mg g<sup>-1</sup> from BC B, and 0.06 mg g<sup>-1</sup> from BC C. Similar results were observed for biochars produced from corn stovers (Hollister et al. 2013). Compared to the unimpregnated biochars, results showed decreased extractability of phosphates from Fe-impregnated biochars. Quantification confirmed in all three cases, concentrations <0.05 mg g<sup>-1</sup> of released PO<sub>4</sub><sup>3-</sup> and thus potential replacement of weak bound phosphates by nitrates in hydrolysis process on biochar surfaces. This hypothesis was supported by total P contents determination which revealed several times lower P concentrations in impregnated biochar samples. Similar results for

readily soluble anions (PO<sub>4</sub><sup>3-</sup> and NO<sub>3</sub><sup>-</sup>) were published by Wang et al. (2015).

The morphology of the unimpregnated and Fe-impregnated biochar samples was analyzed by using SEM with magnification 250× and mainly showed structures characteristic for the respective input material (Figs. 1–3). Micro-imaging of corn cob-derived biochar (BC A) before and after Fe impregnation (Fig. 1a, b) illustrates clogging or filling of empty micro- and mesopores by iron particles. Additionally, structures after impregnation and thus acid hydrolysis showed destroyed pore walls and layers. EDX with Fe surface mapping of impregnated biochar particles (Fig. 1c, d) confirmed the iron localization and content not in significant concentrations compared to impregnated garden wood waste-derived biochar (Fig. 2c) and wood chip-derived biochar (Fig. 3c), where more stable and more extensive covers of Fe were found. The enormous precipitates of Ca in the form of grains or crystals (Fig. 2a) observed in the case of garden wood waste-derived biochar (BC B) described in details in our previous paper (Frišták et al. 2015) were destroyed after impregnation process and dissolved in acidic reaction solution. The higher content of Ca was confirmed also by comparison EDX spectra of BC B and IBC C (data not shown). Wood chip-derived biochar (BC C) and its impregnated form (IBC C) showed a similar trend as BC B. Acid hydrolysis caused collapse and disturbances of carbon layers and pore walls and subsequent successful impregnation and creation of coherent iron areas orientated more on biochar external surfaces (Fig. 3c).

The spectral analysis in the infrared region which belongs to the most important biochar structural qualitative and semiqualitative analyses (De la Rosa et al. 2014) showed a

**Fig. 1** SEM pictures of unimpregnated BC A (a) and impregnated IBC A (b) biochars at magnification 250 $\times$ . EDX spectrum of impregnated IBC A (c) and EDX element mapping of Fe on impregnated IBC A (d)-scanned region denoted by the yellow box on b. The scanned areas represent the average regions found out as major notable



difference in typical shapes and peaks of biochar samples after Fe impregnation (Fig. 4a–c). Obtained spectra confirmed the similarity in variety of functional groups of BC A, BC B, and BC C. The broad peaks appearing in the spectra of all biochars before and also after impregnation process at around 3600–3300  $\text{cm}^{-1}$  are assigned to O–H vibrations (De la Rosa et al. 2014). The crucial contrasts in FTIR spectra of unimpregnated and impregnated biochars were focused on wavenumbers in range from 1750 to 1250  $\text{cm}^{-1}$ . Comparisons of BC A and IBC A FTIR spectrum (Fig. 4a) revealed changes in intensity of peaks appearing at 1740  $\text{cm}^{-1}$  attributed to C=O stretching vibrations of ketones and carboxylic acids. The significant changes in absorption bands were found out at 1284  $\text{cm}^{-1}$

attributed to C–O stretching vibration of acetyl esters and O–H plane deformation (Kloss et al. 2012). A most intensive peak appeared after Fe impregnation at 1579  $\text{cm}^{-1}$  which is primarily caused by stretching vibrations of double bond in C=C and C=O functional groups of aryls (Chia et al. 2012). Wu et al. (2012) revealed the formation and subsequently vibrations of C=C groups in biochar samples as a main effect of heat-induced cellulose dehydration. Zhao et al. (2013) showed this characteristic peak as a crucial issue to assess the temperature effect on biochar properties. Similar trend showed FTIR spectra of BC B and IBC B (Fig. 4b) with intensive peak at 1430–1440  $\text{cm}^{-1}$  assigned to skeletal C=C vibrations (Zhao et al. 2013). Kloss et al. (2012) revealed this

**Fig. 2** SEM pictures of unimpregnated BC B (a) and impregnated IBC B (b) biochars at magnification 250 $\times$ . EDX spectrum of impregnated IBC B (c) and EDX element mapping of Fe on impregnated IBC B (d)-scanned region denoted by the yellow box on b. The scanned areas represent the average regions found out as major notable

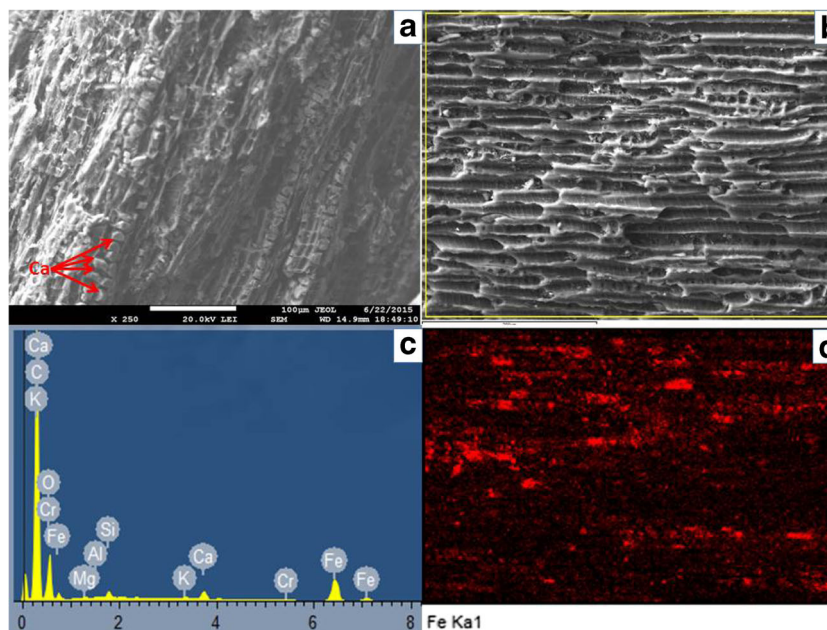
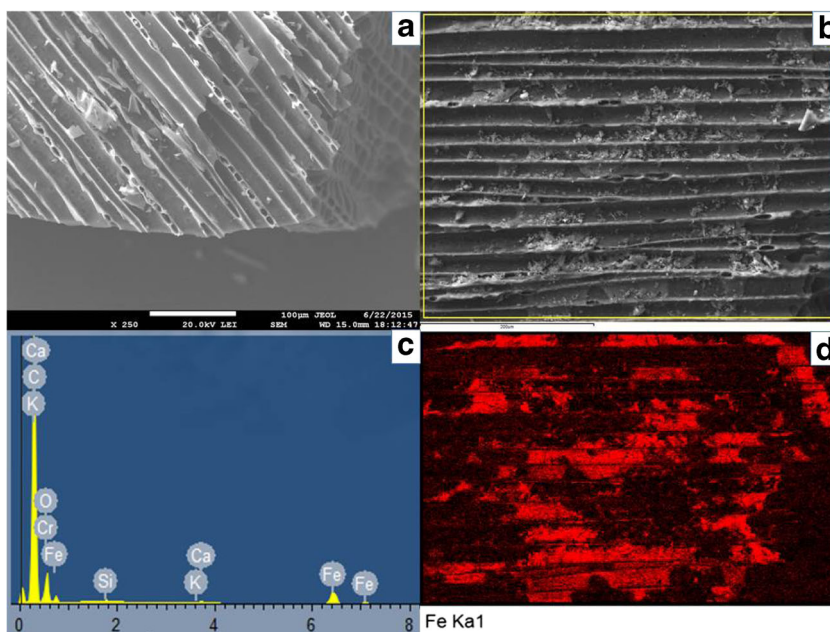


**Fig. 3** SEM pictures of unimpregnated BC C (a) and impregnated IBC C (b) biochars at magnification 250×. EDX spectrum of impregnated IBC C (c) and EDX element mapping of Fe on impregnated IBC C (d)-scanned region denoted by the yellow box on b. The scanned areas represent the average regions found out as major notable



vibration bands in FTIR spectra of poplar and straw biochar and attributed it to aromatic skeletal vibrations combined with C-H in plane deformation or asymmetric C-O stretch of C-O stretching vibrations in carbonates. This information is consistent with highest carbonates content in BC B sample (Table 1). The most obvious changes in intensity of absorption peaks before and after impregnation were found in IBC C (Fig. 4c). The FTIR spectra revealed a band characteristic for wood-derived biochar at 1738  $\text{cm}^{-1}$  assigned to C=O vibrations of ketones and carboxylic acids and 1435  $\text{cm}^{-1}$  assigned to C=C skeletal vibrations (Kloss et al. 2012). The most significant change in intensity of absorption band after impregnation (IBC C) was found in vibration area of C=C and C=O groups around 1560–1575  $\text{cm}^{-1}$  (Keiluweit et al. 2010). Hu et al. (2015) showed the similar changes in absorption intensity of band at 1577  $\text{cm}^{-1}$  assigned to C=O vibrations in hickory chip-derived biochar after Fe impregnation process.

**Sorption kinetics**

Sorption experiments showed minimal sorption of  $\text{PO}_4^{3-}$  by unimpregnated BC A, BC B, and BC C (Fig. 5a) and thus a strong effect of surface negative charge of biochar and repulsion of anionic chemical forms was confirmed (Janus et al. 2015). However, the Fe impregnation showed significant positive effect on sorption capacity for all three studied biochar-based sorbents (Fig. 5b). Kinetic studies of  $\text{PO}_4^{3-}$  sorption processes from single-component system by the three biochars before and after impregnation pointed to two-phase processes occurring in initially rapid sorption during the first 2 h and then slower uptake till reaching the sorption equilibrium in 24 h. The first step could be attributed to rapid occupation of easily accessible external surface sorption sites (Frišták

et al. 2015). Residual sites with lower affinity are occupied slowly and this phase could be related to the formation of inner layer complexes or by slow diffusion into pores (Remenárová et al. 2014). The obtained sorption data from kinetic studies were fitted and described by mathematical equations of pseudo-first, pseudo-second, and pseudo-*n*th order kinetic model (Fig. 5a, b). Kinetic parameters obtained by the non-linear regression analysis are shown in Table 2. Based on the coefficients of determination  $R^2$ , it is evident that the pseudo-*n*th order model was the most efficient for evaluation and describing sorption kinetics of phosphates for all unimpregnated and impregnated sorbents.

**Sorption isotherms**

The modeling of sorption equilibrium offers valuable information for better evaluation of sorption system. The sorption data of phosphate separation from a single-component system by unimpregnated BC A, BC B, and BC C and Fe-impregnated IBC A, IBC B, and IBC C showed adsorption isotherms of a typical “L” shape. For the study of phosphate equilibrium sorption onto unimpregnated and impregnated biochars, the models of Langmuir (Eq. 6), Freundlich (Eq. 7), and DKR (Eq. 8) adsorption isotherms were applied.

Model parameters obtained from non-linear regression analysis are presented in Table 3. The comparison of  $R^2$  values of models applied for fitting of  $\text{PO}_4^{3-}$  sorption data by BC A and BC B showed higher efficiency of DKR model application compared to Langmuir and Freundlich adsorption models. On the other hand, evaluation of BC C, IBC A, IBC B, and IBC C sorption parameters showed better suitability of Langmuir and Freundlich models compared to the DKR model. Our previous work

**Fig. 4** FTIR spectra of unimpregnated and Fe-impregnated BC A and IBC A (a), BC B and IBC B (b), and BC C and IBC C (c). Vertical dashed lines mean main observed peaks

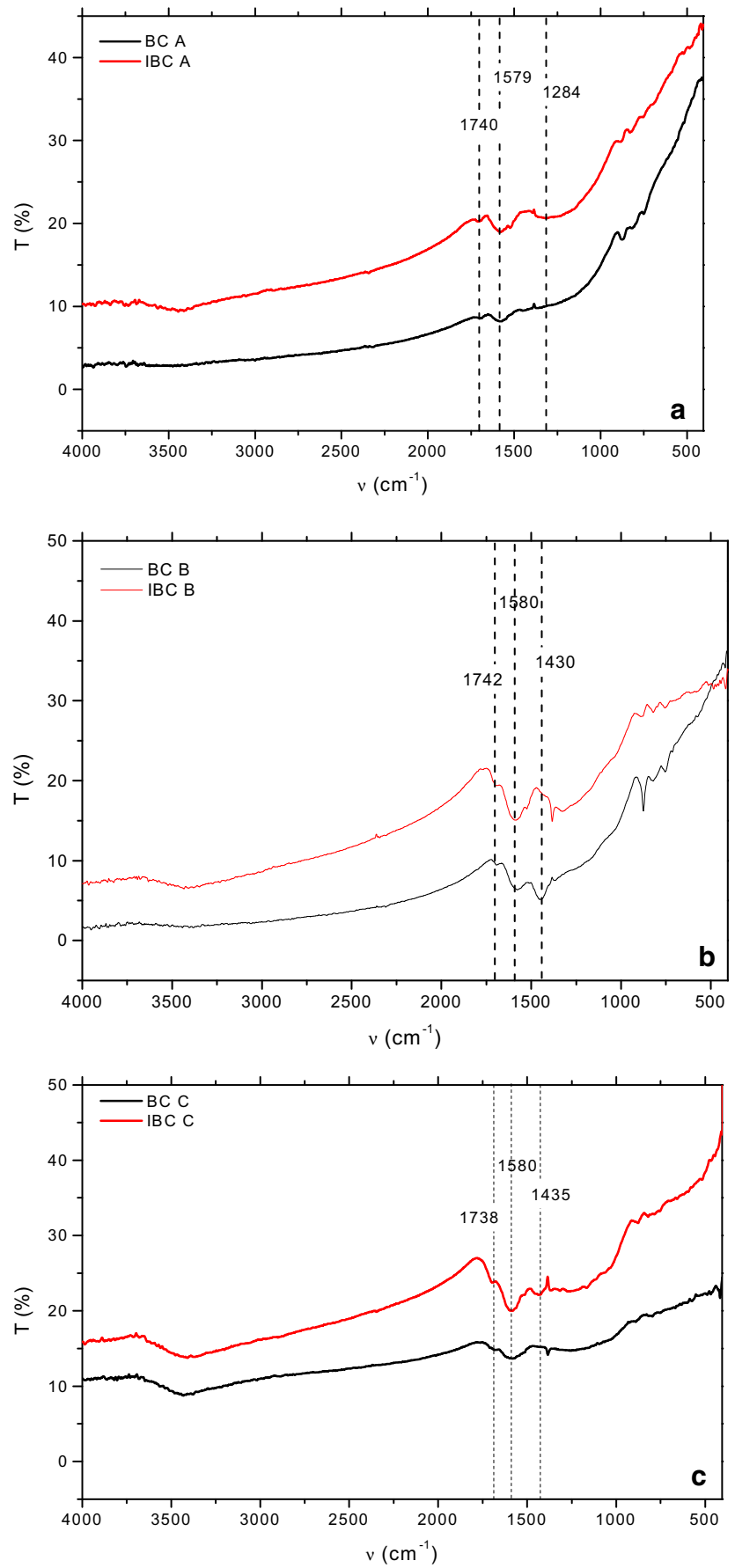
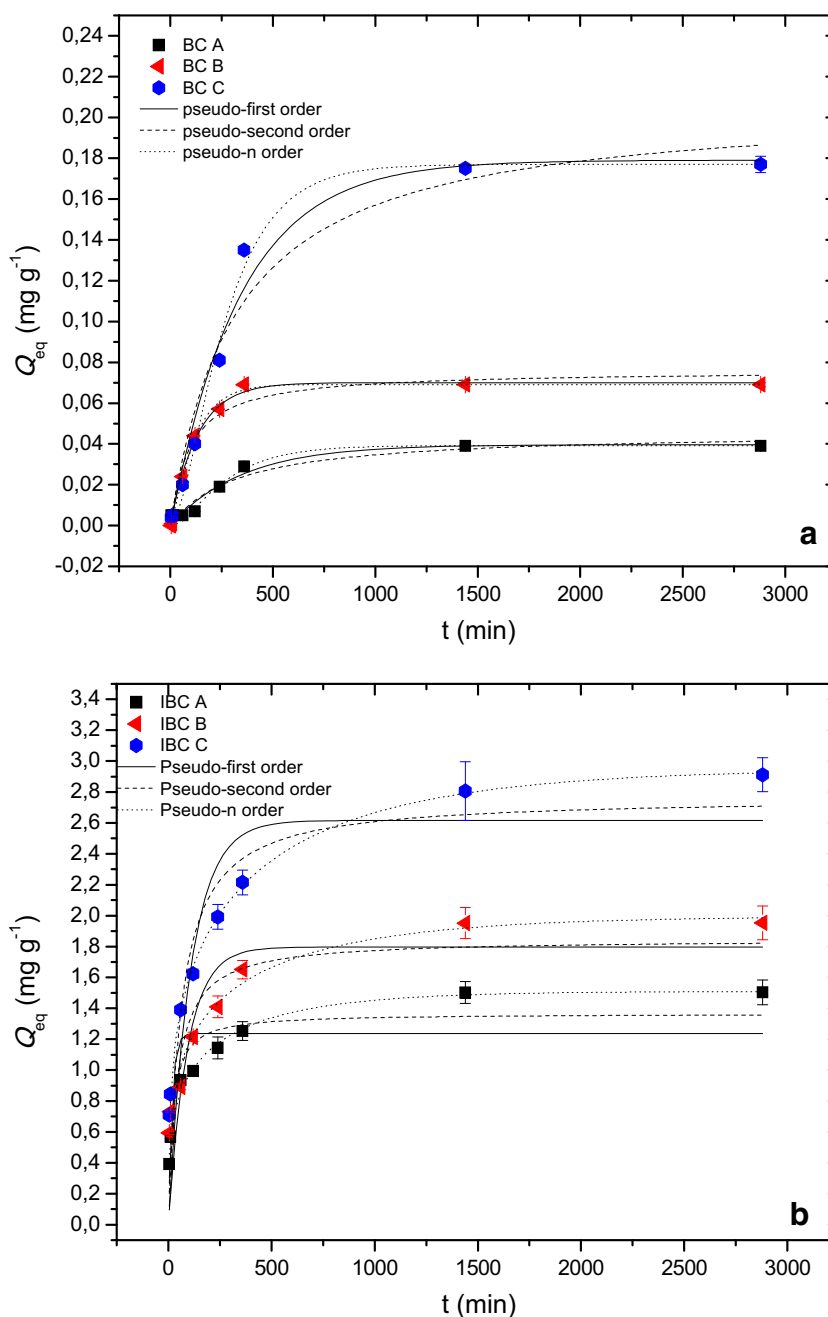




**Fig. 5** Effect of contact time on sorption capacity of BC A (corn cob-derived biochar), BC B (garden wood rest-derived biochar), and BC C (wood chip-based biochar) (a) and IBC A (Fe-impregnated BC A), IBC B (Fe-impregnated BC B), and IBC C (Fe-impregnated BC C) (b) for  $\text{PO}_4^{3-}$  ions. Conditions are as follows: sorbent  $33.3 \text{ g L}^{-1}$ ;  $c_0 \text{ PO}_4^{3-} 61.3 \text{ mg L}^{-1}$ ; pH  $5.65 \pm 0.1$ ; and time periods 5, 10, 60, 120, 240, 360, 1440, and 2880 min



(Frišták et al. 2015) pointed out the applicability of DKR equation in lower  $c_{eq}$  region of studied sorbates. The values of Langmuir  $Q_{max}$  for all unimpregnated and impregnated sorbents were higher than values of DKR  $Q_m$  which is related to the total specific micropore volume of the biochar sorbents. The calculated values of Langmuir  $Q_{max}$  decreased in order BC C > BC B > BC A for unimpregnated biochars, and in order IBC C > IBC B > IBC A for Fe-impregnated biochars. Additionally, the parameter  $b$  that is related to the affinity of the binding sites (Krajňák et al. 2015) allows the comparison of the sorbent affinities towards the phosphates. Sorption

affinity decreased in order BC B > BC C > BC A for unimpregnated sorbents and IBC B > IBC A > IBC C for Fe-impregnated sorbents. Generally, Fe impregnation increased sorption capacities of studied biochar-based sorbents for phosphates by more than 55 times for BC A, 20 times for BC B, and 12 times for BC C. Improved sorption capacities of impregnated materials could be related to observations of main structural and morphological changes in materials. The values of SA and AEC correlate with obtained  $Q_{max}$  values. Rapid increase in total Fe concentration after impregnation process caused increase in concentration of new reaction sorption sites for anionic

**Table 2** Pseudo-first, pseudo-second, and pseudo-*n*th rate constants for sorption process of PO<sub>4</sub><sup>3-</sup> by BC A, BC B, BC C, IBC A, IBC B, and IBC C

Sorbent	Pseudo-first order rate constants			Pseudo-second order rate constants			Pseudo- <i>n</i> th order rate constants		
	$Q_{eq}$ (mg g <sup>-1</sup> )	$k_1$ (min <sup>-1</sup> )	$R^2$	$Q_{eq}$ (mg g <sup>-1</sup> )	$k_2$ (g mg <sup>-1</sup> min <sup>-1</sup> )	$R^2$	$Q_{eq}$ (mg g <sup>-1</sup> )	$k_n$ (g mg <sup>-1</sup> min <sup>-1</sup> )	$R^2$
BC A	0.039	0.003	0.957	0.046	0.066	0.941	0.039	0.035	0.965
BC B	0.070	0.004	0.992	0.076	0.039	0.968	0.069	0.014	0.994
BC C	0.179	0.003	0.885	0.208	0.015	0.868	0.177	0.006	0.911
IBC A	1.238	0.055	0.749	1.366	0.036	0.888	1.509	0.003	0.989
IBC B	1.797	0.011	0.764	1.846	0.013	0.872	1.995	0.002	0.981
IBC C	2.616	0.009	0.752	2.765	0.006	0.867	2.951	0.001	0.999

species in all materials. However, SEM analysis showed the effect of hydrolysis and subsequent blocking porous structures and wall destroying which can make unavailable Fe-containing sorption sites. The EDX analysis with Fe mapping on IBC A, IBC B, and IBC C particles showed the most intensive Fe composites on BC C surfaces able to bind free anions from solution. Hu et al. (2015) found strong sorption ability of Fe-impregnated biochar to aqueous As removal with Langmuir maximum sorption capacity of 2.16 mg g<sup>-1</sup>. The authors discussed chemisorption as a main sorption mechanism of As removal by Fe-impregnated biochar. Additionally, they suggested a main role for O-containing functional groups, whose concentration after impregnation increased. Because of comparable ionic structure of arsenate and phosphate, we can expect similar sorption mechanisms.

Based on these results, we suppose that the creation and formation of new surface binding sites related to Fe<sub>2</sub>O<sub>3</sub> with saturation by easily releasable NO<sub>3</sub><sup>-</sup> ions played a crucial role for improving the sorption capacities of Fe-impregnated biochars. This hypothesis was confirmed also by elemental analysis of total N content in impregnated samples (Table 1).

The highest concentration and therefore the most significant effect of nitrates content was found in impregnated wood chip-derived biochar sample. Subsequent ion exchange of nitrates and phosphates is considered as a main chemisorption mechanism in case of Fe-impregnated biochars. The observed  $Q_{max}$  values of the studied impregnated sorbents for phosphates are comparable with various biochar-based sorbents developed by other working groups (Table 4). The sorption behavior of impregnated sorbents and easy-going process

**Table 3** Langmuir, Freundlich, and DKR equilibrium parameters (±SD) for PO<sub>4</sub><sup>3-</sup> ion sorption by BC A, BC B BC C, IBC A, IBC B, and IBC C obtained by non-linear regression analysis

Sorbent	Model	$Q_{max}$ (mg g <sup>-1</sup> )	$b$ (L mg <sup>-1</sup> )	$K$ (L g <sup>-1</sup> )	$1/n$	$Q_m$ (mg g <sup>-1</sup> )	$\beta$ (mol <sup>2</sup> J <sup>-2</sup> )	$R^2$
BC A	Langmuir	0.036 ± 0.001	0.984 ± 0.021	–	–	–	–	0.984
	Freundlich	–	–	0.008 ± 0.001	0.649 ± 0.014	–	–	0.955
	DKR	–	–	–	–	0.021 ± 0.001	3.621 × 10 <sup>-4</sup>	0.988
BC B	Langmuir	0.132 ± 0.007	0.013 ± 0.001	–	–	–	–	0.968
	Freundlich	–	–	0.007 ± 0.001	0.514 ± 0.015	–	–	0.905
	DKR	–	–	–	–	0.094 ± 0.005	2.616 × 10 <sup>-4</sup>	0.991
BC C	Langmuir	0.269 ± 0.008	0.016 ± 0.001	–	–	–	–	0.984
	Freundlich	–	–	0.019 ± 0.002	0.456 ± 0.014	–	–	0.951
	DKR	–	–	–	–	0.166 ± 0.001	1.434 × 10 <sup>-5</sup>	0.731
IBC A	Langmuir	1.988 ± 0.142	0.033 ± 0.015	–	–	–	–	0.971
	Freundlich	–	–	0.244 ± 0.011	0.393 ± 0.014	–	–	0.994
	DKR	–	–	–	–	1.460 ± 0.012	9.987 × 10 <sup>-6</sup>	0.886
IBC B	Langmuir	2.754 ± 0.085	0.017 ± 0.001	–	–	–	–	0.953
	Freundlich	–	–	0.193 ± 0.008	0.473 ± 0.007	–	–	0.995
	DKR	–	–	–	–	1.624 ± 0.097	1.636 × 10 <sup>-5</sup>	0.828
IBC C	Langmuir	3.201 ± 0.187	0.211 ± 0.004	–	–	–	–	0.995
	Freundlich	–	–	1.510 ± 0.112	0.159 ± 0.076	–	–	0.970
	DKR	–	–	–	–	2.989 ± 0.147	5.123 × 10 <sup>-6</sup>	0.604

**Table 4** Maximum sorption capacity ( $Q_{max}$ ) of selected biochar-based sorbents for  $PO_4^{3-}$  ions

Sorbent	Feedstock	Modification	$Q_{max}$ (mg g <sup>-1</sup> )	Reference
IBC A	Corn cobs	Fe impregnation	1.99 ± 0.03	This paper
IBC B	Garden wood waste	Fe impregnation	2.75 ± 0.02	This paper
IBC C	Wood chips	Fe impregnation	3.20 ± 0.21	This paper
MOP400	Orange peel	Fe <sup>3+</sup> /Fe <sup>2+</sup> co-precipitation	0.22 ± 0.16	Chen et al. 2011
MOP700	Orange peel	Fe <sup>3+</sup> /Fe <sup>2+</sup> co-precipitation	1.24 ± 0.02	Chen et al. 2011
TC500	<i>Thaliadealbata</i>	CO <sub>2</sub> activation	2.54 ± 0.25	Zeng et al. 2013
TC600	<i>Thaliadealbata</i>	CO <sub>2</sub> activation	2.86 ± 0.28	Zeng et al. 2013

preparation predetermine this chemical modification as crucial for the processing of improved sorption materials.

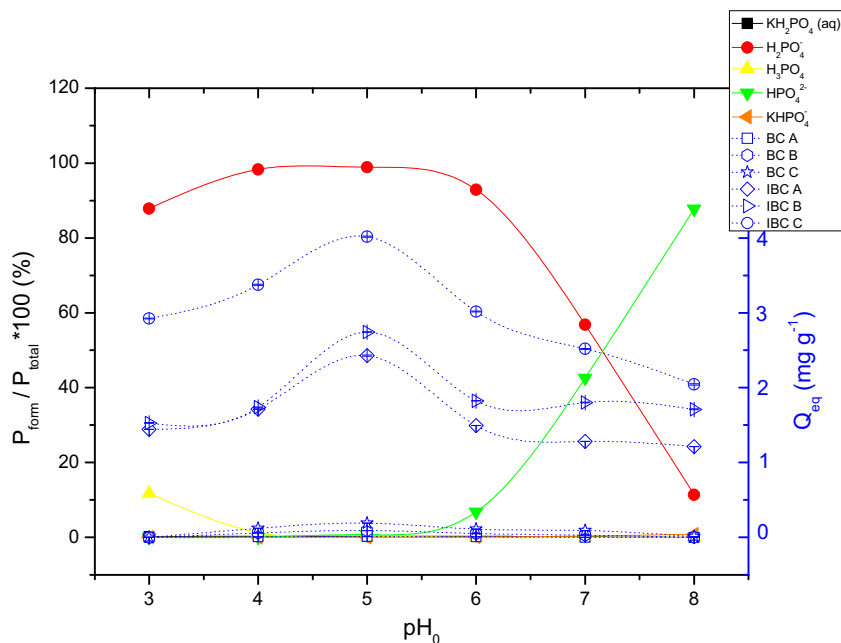
**Effect of pH on phosphate sorption**

The pH effect is one of the most important parameters for the evaluation of biochar sorption properties (Bogusz et al. 2015). Depending on the element, pH affects the charge of sorbent surfaces, the level of element ionization and thus the formation of new speciation forms (Remenárová et al. 2012). In aqueous solution, phosphate exists as several species, whose concentration is controlled by solution pH and present of other element forms in system.

Generally, P exists as  $H_3PO_4$ ,  $H_2PO_4^-$ ,  $HPO_4^{2-}$ , and  $PO_4^{3-}$ . At pH 2, P exists as neutral species which is weakly attached to the sites of sorption materials (Kumar et al. 2010). At higher pH, more interactive P-forms are formed. Variety of P-speciation forms in reaction solution dependent on pH was confirmed by in silico speciation analysis (Fig. 6), calculated for the studied reaction conditions. We found that at pH 4.5–5.5 most of P was present in the reaction solution as diprotic

acid  $H_2PO_4^-$  (>95 %). At higher pH, the concentrations of other chemical forms such as  $HPO_4^{2-}$  increased. Sorption experiments showed that sorption processes of phosphates by all unimpregnated and impregnated biochars depended on initial pH value (Fig. 6). The sorption capacities of IBC A, IBC B, and IBC C increased with increasing of initial pH value in the range 3–5 and subsequently decreased in the range 6–8. This result is consistent with the proposed sorption mechanism and determination of optimum sorption pH around 5, at which almost all phosphates exist in the form of  $H_2PO_4^-$ . The obtained results offer a new dimension for study of sorption interactions between biochar and phosphates based on reaction pH and thus clarification of electrostatic interactions as an important mechanism in phosphates removal process. In the works of Zhang et al. (2012) and Wang et al. (2015), information about reaction pH of phosphate sorption experiments were missing. On the other hand, Yao et al. (2011) described similar mechanisms and pH effects on  $PO_4^{3-}$  sorption removal by biochar derived from anaerobically digested sugar beet tailings. Authors showed the increasing sorption of phosphates by biochar in the pH range from 2 to 4.1 and

**Fig. 6** Effect of initial pH on the sorption of P (150 mg L<sup>-1</sup>  $PO_4^{3-}$ ) by BC A, BC B, BC C, IBC A, IBC B, and IBC C (33.3 g L<sup>-1</sup>) from single-component sorption system and theoretical phosphorus speciation in reaction solution calculated by Visual MINTEQ ver. 3.0 with the following initial conditions: 150 mg L<sup>-1</sup>  $PO_4^{3-}$  in form of  $KH_2PO_4$ ,  $T = 24\text{ }^\circ\text{C}$ ,  $pCO_2 = 38.5\text{ Pa}$



highlighted pH 5.2 as an optimum pH for phosphate removal. At higher than optimum pH, polynuclear interactions may be triggered and may consume more adsorption sites.

## Conclusion

Impregnated biochar-based sorbents were tested for sorption capacity of phosphates from single-component aqueous system compared to unimpregnated biochars. The highest sorption capacity of phosphate  $Q_{max}$   $3.201 \pm 0.187$  mg g<sup>-1</sup> for Fe-impregnated wood chip-derived biochar was determined. Our study confirmed the dependence of PO<sub>4</sub><sup>3-</sup> sorption by impregnated sorbents on reaction pH, contact time, and initial concentration of phosphorus in solution. Based on micro-imaging (SEM-EDX) and low Fe concentration found in filtrates, we confirmed that Fe was well retained in the biochar and thus negatively charged phosphate species were attracted through electrostatic forces to positively charged functional groups on the surface of biochar. Because of its low cost and fast preparation, this engineered biochar could be used as an alternative remediation sorbent for anionic contaminants such as PO<sub>4</sub><sup>3-</sup> or H<sub>2</sub>AsO<sub>4</sub><sup>-</sup>.

**Acknowledgments** The authors Vladimír Frišták and Gerhard Soja thank the Austrian FFG for the financial support of the Research Studio FERTI-MINE, project no. 844744. Libor Ďuriška would like to thank the project implementation: Center for development and application of advanced diagnostic methods in processing of metallic and non-metallic materials, ITMS: 26220120014, supported by the Research and Development Operational Programme funded by the ERDF.

## References

- Agrafioti E, Kalderis D, Diamadopoulos E (2014) Ca and Fe modified biochars as adsorbents of arsenic and chromium in aqueous solutions. *J Environ Manag* 146:444–450
- Ahmad M, Rajapaksha AU, Lim JE, Zhang M, Bolan N, Mohan D, Vithanage M, Lee SS, Ok YS (2014) Biochar as a sorbent for contaminant management in soil and water: a review. *Chemosphere* 99:19–33
- Azizian S, Fallah RN (2010) A new empirical rate equation for adsorption kinetics at solid/solution interface. *Appl Surf Sci* 256:5153–5156
- Bogusz A, Oleszczuk P, Dobrowolski R (2015) Application of laboratory prepared and commercially available biochars to adsorption of cadmium, copper and zinc ions from water. *Bioresour Technol* 196:540–549
- Borchard N, Wolf A, Laabs V, Aeckerberg R, Scherer HW, Moeller A, Amelung W (2012) Physical activation of biochar and its meaning for soil fertility and nutrient leaching—a greenhouse experiment. *Soil Use Manage* 28:177–184
- Chen B, Chen Z, Li S (2011) A novel magnetic biochar efficiently sorbs organic pollutants and phosphate. *Bioresour Technol* 102:716–723
- Chia CH, Gong B, Joseph SD, Marjo CE, Munroe P, Rich AM (2012) Imaging of mineral-enriched biochar by FTIR, Raman and SEM-EDX. *Vib Spectrosc* 62:248–257
- De La Rosa C, Paneque M, Miller AZ, Knicker H (2014) Relating physical and chemical properties of four different biochars and their application rate to biomass production of *Lolium perenne* on a calcic cambisol during a pot experiment of 79 days. *Sci Total Environ* 499:175–184
- Enders A, Lehmann J (2012) Comparison of wet-digestion and dry-ashing methods for total elemental analysis of biochar. *Commun Soil Sci Plan* 43:1042–1052
- Frišták V, Friesl-Hanl W, Pipiška M, Richveisová-Micháleková B, Soja G (2014) The response of artificial aging to sorption properties of biochar for potentially toxic heavy metals. *Nova Biotechnologica et Chimica* 13:137–147
- Frišták V, Pipiška M, Lesný J, Soja G, Friesl-Hanl F, Packová A (2015) Utilization of biochar sorbents for Cd<sup>2+</sup>, Zn<sup>2+</sup>, and Cu<sup>2+</sup> ions separation from aqueous solutions: comparative study. *Environ Monit Assess* 187:4093
- Galamboš M, Daňo M, Víglašová E, Krivosudský I, Roszkopfová O, Novák I, Berek D, Rajec P (2015) Effect of competing anions on perchlorate adsorption by activated carbon. *J Radioanal Nucl Chem* 304:1219–1224
- Gustafsson JP (2013) Visual-MINTEQ, version 3.0 (computer software). Stockholm, Sweden: Kungliga Tekniska högskolan
- Hollister CC, Bisogni JJ, Lehmann J (2013) Ammonium, nitrate and phosphate sorption to and solute leaching from biochars prepared from corn stover (L.) and oak wood (spp.). *J Environ Qual* 42:137–144
- Hu X, Ding Z, Zimmerman AR, Wang S, Gao B (2015) Batch and column sorption of arsenic onto iron-impregnated biochar synthesized through hydrolysis. *Water Res* 68:206–216
- Janus A, Pelfréne A, Heymans S, DeboffeCh DF, Waterlot C (2015) Elaboration, characteristics and advantages of biochars for the management of contaminated soils with a specific overview on miscanthus biochars. *J Environ Manag* 162:275–289
- Keiluweit M, Nico PS, Johnson MG, Kleber M (2010) Dynamic molecular structure of plant biomass-derived black carbon (biochar). *Environ Sci Technol* 44:1247–1253
- Kloss S, Zehetner F, Dellantonio A, Hamid R, Ottner F, Liedtke V, Schawanninger M, Gerzabek MH, Soja G (2012) Characterization of slow pyrolysis biochars: effects of feedstocks and pyrolysis temperature on biochar properties. *J Environ Qual* 41:990–1000
- Kolodynska D, Wnetrzak R, Leahy JJ, Hayes MBH, Kwapinski W, Hubicki Z (2012) Kinetic and adsorptive characterization of biochar in metal ions removal. *Chem Eng J* 197:295–305
- Krajňák PL, Roszkopfová O, Galamboš M, Rajec P (2015) Adsorption of nickel on rhyolitic Slovak bentonites. *J Radioanal Nucl Chem* 304:587–593
- Kumar P, Sudha S, Chand S, Srivastava VC (2010) Phosphate removal from aqueous solution using coir-pith activated carbon. *Separ Sci Technol* 45:1463–1470
- Laird DA, Fleming P, Davis DD, Horton R, Wang BQ, Karlen DL (2010) Impact of biochar amendments on the quality of a typical Midwestern agricultural soil. *Geoderma* 158:443–449
- Lawrinenko M (2014) Anion exchange capacity of biochar. Graduate Theses and Dissertations Paper:13685
- Lehmann J, Joseph S (2015) Biochar for environmental management: science, technology and implementation. Earthscan from Routledge, London 944 pp
- Martin SM, Kookana RS, Van Zwieten L, Krull E (2012) Marked changes in herbicide sorption-desorption upon ageing of biochars in soil. *J Hazard Mater* 231–232:70–78
- Moreno-Castilla C (2004) Adsorption of organic molecules from aqueous solutions on carbon materials. *Carbon* 42:83–94
- Novak JM, Busscher WJ, Laird DL, Ahmedna M, Watts DW, Niandou MA (2009) Impact of biochar amendment on fertility of a southeastern coastal plain soil. *Soil Sci* 174:105–112



- Nunes CA, Guerreiro MC (2011) Estimation of surface area and pore volume of activated carbons by methylene blue and iodine numbers. *Quim Nov* 34:472–476
- Puschenreiter M, Wittstock F, Friesl-Hanl W, Wenzel W (2013) Predictability of the Zn and Cd phytoextraction efficiency of a *Salix Smithiana* clone by DGT and conventional bioavailability assays. *Plant Soil* 369:531–541
- Remenárová L, Pipiška M, Horník M, Rozložník M, Augustín J, Lesný J (2012) Biosorption of cadmium and zinc by activated sludge from single and binary solutions: mechanism, equilibrium and experimental design study. *J Taiwan Inst Chem Eng* 43:433–443
- Remenárová L, Pipiška M, Florková E, Horník M, Rozložník M, Augustín J (2014) Zeolites from coal fly ash as efficient sorbents for cadmium ions. *Clean Technol Environ* 16:1551–1564
- Sharpley A, Foy B, Withers P (2000) Practical and innovative measures for the control of agricultural phosphorus losses to water: an overview. *J Environ Qual* 29:1–9
- Tang J, Zhu W, Kookana R, Katayama A (2013) Characteristics of biochar and its application in remediation of contaminated soil. *J BiosciBioeng* 116:653–659
- Wang Z, Guo H, Shen F, Yang G, Zhang Y, Zeng Y, Wang L, Xiao H, Deng S (2015) Biochar produced from oak sawdust by lanthanum (La)-involved pyrolysis for adsorption of ammonium ( $\text{NH}_4^+$ ), nitrate ( $\text{NO}_3^-$ ), and phosphate ( $\text{PO}_4^{3-}$ ). *Chemosphere* 119:646–653
- Wu W, Yang M, Feng Q, McGrouther K, Wang H, Lu H (2012) Chemical characterization of rice straw-derived biochar for soil amendment. *Biomass Bioenerg* 47:268–276
- Yao Y, Gao B, Inyang M, Zimmerman AR, Cao XD, Pullammanappallil P, Yang LY (2011) Removal of phosphate from aqueous solution by biochar derived from anaerobically digested sugar beet tailings. *J Hazard Mater* 190:501–507
- Zeng Z, Zhang SD, Li TQ, Zhao FL, He ZL, Zhao HP, Yang X, Wang HL, Zhao J, Rafiq MT (2013) Sorption of ammonium and phosphate from aqueous solution by biochar derived from phytoremediation plants. *J Zhejiang Univ Sci B* 14:1152–1161
- Zhang M, Gao B (2013) Removal of arsenic, methylene blue and phosphate by biochar/AlOOH nanocomposite. *Chem Eng J* 130:457–462
- Zhang M, Gao B, Yao Y, Xue Y, Inyang M (2012) Synthesis, characterization, and environmental implications of graphene-coated biochar. *Sci Total Environ* 435–436:567–572
- Zhao L, Cao X, Mašek O, Zimmerman A (2013) Heterogeneity of biochar properties as a function of feedstock sources and production temperatures. *J Hazard Mater* 256–257:1–9